We are IntechOpen, the world's leading publisher of Open Access books
Built by scientists, for scientists

6,900
Open access books available

185,000
International authors and editors

200M
Downloads

154
Countries delivered to

Our authors are among the

TOP 1%
most cited scientists

12.2%
Contributors from top 500 universities

CLARIVATE ANALYTICS
BOOK CITATION INDEX
INDEXED

WEB OF SCIENCE™

Selection of our books indexed in the Book Citation Index
in Web of Science™ Core Collection (BKCI)

Interested in publishing with us?
Contact book.department@intechopen.com

Numbers displayed above are based on latest data collected.
For more information visit www.intechopen.com

Cathodoluminescence Properties of SiO$_2$: Ce^{3+},Tb^{3+}, SiO$_2$:Ce^{3+}, Pr^{3+} and SiO$_2$: PbS

Odireleng M. Ntwaeaborwa[1], Gugu H. Mhlongo[1,2], Shreyas S. Pitale[1],
Mokhotswa S. Dhlamini[1,3], Robin E. Kroon[1] and Hendrik C. Swart[1]
[1]Department of Physics, University of the Free State, Bloemfontein
[2]National Centre for Nanostructured Materials, CSIR, Pretoria
[3]Department of Physics, University of South Africa, Pretoria
South Africa

1. Introduction

Silicon dioxide (SiO$_2$), also known as silica, is an oxide of silicon (Si) that is found in nature in two different forms, namely amorphous and crystalline. Traditionally, amorphous SiO$_2$ is used in many applications such as semiconductor circuits, microelectronics and optical fibers for telecommunication. In modern age research, amorphous glassy SiO$_2$ has emerged as a potential host lattice for a variety of rare-earth ions to prepare light emitting materials or phosphors that can be used in different types of light emitting devices. SiO$_2$ based phosphors can also be prepared by encapsulating semiconducting nanocrystals of zinc oxide (ZnO) and lead sulphide (PbS). In addition, recent studies have demonstrated that when semiconducting nanocrystals are incorporated in glassy SiO$_2$ activated with trivalent rare earth ions (Ce^{3+},Tb^{3+},Eu^{3+},Pr^{3+}) light emission from the rare-earth luminescent centres could be increased considerably as a result of energy transfer from the nanocrystals to the rare-earths, i.e. semiconducting nanocrystals act as sensitizers for radiative relaxation processes in these centres.

Like any other oxide, amorphous SiO$_2$ is expected to be a good host matrix for rare-earth ions for preparation of phosphors because oxides are more chemically stable than traditional sulphide matrices. In addition, SiO$_2$ has been reported to have advantages such as high transparency, dopant solubility and ease of production (Nogami et al., 2007; Ntwaeaborwa et al., 2007,2008). In recent studies, the preparation of phosphors by incorporation of semiconducting nanocrystals and rare-earths ions in amorphous SiO$_2$ has commonly been achieved by using a sol-gel method. This method has been reported to have more advantages over other wet chemistry and conventional glass processing methods because of its potential to produce materials with high purity and homogeneity at low temperatures (Hench & West, 1990; Ding, 1991). It extends the traditional glass melting processes by allowing incorporation of semiconductor nanocrystals and rare-earth activators at low temperatures and predetermined concentrations in such a way that the size and shape of the particles can be controlled (Reisfeld, 2000) during nucleation and growth processes. The sol-gel method was used in this study to prepare respectively red, green and blue cathodoluminescent phosphors by incorporating trivalent rare-earth ions such as

prasedomium (Pr^{3+}), terbium (Tb^{3+}) and cerium (Ce^{3+}) in amorphous SiO_2. Orange-red cathodoluminescence was also observed when PbS nanocrystals were incorporated in the sol-gel derived SiO_2. Cathodoluminescence intensity of these phosphors was shown to increase either by co-doping with a different rare-earth ion or encapsulating ZnO nanocrystals.   The CL properties and the intensity degradation of these SiO_2 based phosphors were evaluated for their possible application in low voltage cathodoluminescent flat panel displays such as field emission displays (FEDs) and plasma display panels (PDPs).

This chapter is a review of cathodoluminescent properties of phosphor materials prepared by incorporating Ce^{3+}, Tb^{3+}, Pr^{3+} and PbS nanocrystal in amorphous SiO_2 host. The effects of rare-eaths co-doping and encapsulating of ZnO nanocrystals on cathodoluminescent intensity of these materials is also presented. In addition, a review of cathodoluminescence intensity degradation when these phosphors were irradiated with a beam of electron is discussed. It was demonstrated that when these phosphors were irradiated with the beam of electrons for a long period of time they lose their CL intensity and this occured simultaneously with desorption of oxygen (O) from the phosphor surfaces. In the process, an oxygen deficient non-luminescent layer was formed on the surface whose formation could be explained by an electron stimulated surface chemical reaction (ESSCR) model proposed by Holloway and co-workers (Holloway et al., 1996, 2000). The desorption of atomic species was explained by Knotek-Fiebelman electron stimulated desorption (ESD) proposed by Knotek and Feibelman (Knotek and Feibelman, 1978). The objective of the study was to investigate the effects of a prolonged electron beam irradiation, accelerating voltage, and oxygen gas on the CL properties and the chemical stability of these phosphors.

2. Cathodoluminescence intensity degradation

 Cathodoluminescence (CL) degradation can be defined as a process by which cathodoluminescent phosphors, used mainly in cathode ray tubes (CRTs) or field emission display (FEDs), lose their brightness (luminescence intensity) as a result of prolonged irradiation by a beam of electrons during normal operation.   The CL intensity degradation of CRT/FED phosphors, with special reference to traditional sulphide based phosphors, is a well documented phenomenon. When a beam of electrons is incident on a phosphor, a number of physical processes can occur. These include emission of secondary electrons, Auger electrons and back-scattered electrons. Hundreds of free electrons and free holes are produced along the path of the incident electron (primary excitation electrons). As illustrated in figure 1, the free electrons and holes may couple and produce electron-hole (e-h) pairs that can diffuse through the phosphor and transfer their energy to luminescent centres resulting in emission of visible photons (Stoffers, 1996; Raue, 1989). This process is referred to as radiative recombination.   Unwanted processes in which the e-h pairs recombine non-radiatively by transferring their energy to killer centers (incidental impurities and/or inherent lattice defects) are also possible. The e-h pairs can also diffuse to the surface of the phosphor and recombine non-radiatively (Stoffers, 1996). In this case, a non-luminescent oxide layer, which is known to reduce the CL intensity of the CRT/FED phosphors, may form on the surface. For examples, it was demonstrated that when zinc sulfide (ZnS) based phosphors were exposed to a prolonged irradiation by energetic beam of electrons, the ZnS host dissociated into reactive ionic Zn^{2+} and S^{2-} species, which in turn combined with ambient vacuum gases such as O_2 and H_2O to form non-luminescent ZnO or

ZnSO$_4$ layers or H$_2$S gas (Swart el al., 1998; Itoh et al., 1989) as explained by the ESSCR model (Holloway et al., 1996, 2000). In the case of oxide based systems, the electron beam induced dissociation of atomic species is followed by desorption of oxygen from the surface. For example, Knotek and Fiebelman observed desorption of surface oxygen when SiO$_2$ or TiO$_2$ was irradiated with a beam of electrons and they developed a model called Knotek-Fiebelman electron stimulated desorption (ESD) mechanism to explain the desorption process. According to this model, O$^+$ species produced in the valence band of SiO$_2$ (TiO$_2$) desorb from the surface following the creation of an electron-hole pair in the L$_{2,3}$ level of Si, Auger relaxation and emission (Knotek and Feibelman, 1978).
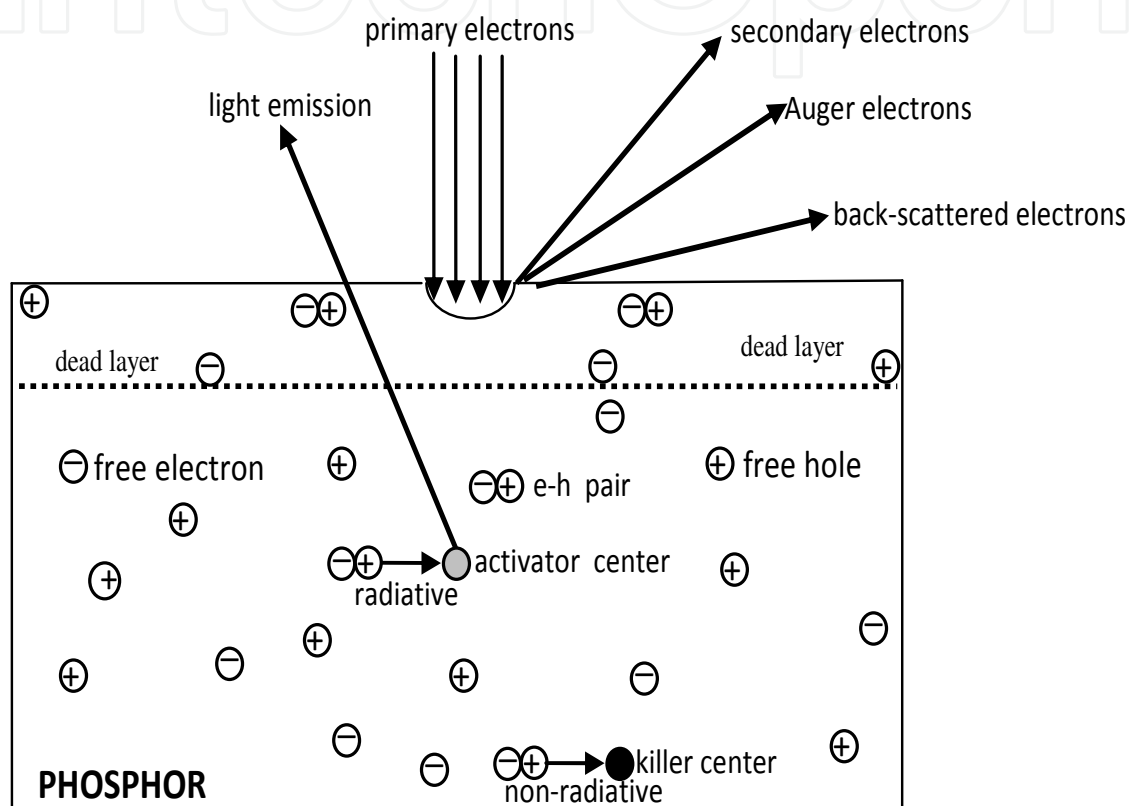
Fig. 1. Cathodoluminescence process in a phosphor grain.

3. Experiments

A sol-gel process was used to prepare rare-earths (Ce^{3+},Tb^{3+},Pr^{3+}) doped and semiconducting nanocrystals (ZnO and PbS) encapsulated SiO$_2$ based phosphors. The sol-gel is a wet chemical technique commonly used to prepare glassy and ceramic materials at low temperatures. It involves the preparation of a viscous solution (sol) from one or more precursor materials and the conversion of the sol into a gel. There are two major chemical reactions integral to the sol-gel process, namely hydrolysis (reaction of metal alkoxides with water to form oxides) and condensation/polymerization (the formation of a three dimensional network). In the presence of a catalyst, the conversion of the sol to gel can be completed in a short time (within ~1-2 hrs). For more information on the sol-gel process, the reader is referred to the literature cited (Hench & West, 1990; Klein, 1985; Huang et al., 1985).

3.1 Preparation of PbS and ZnO nanocrystals

Lead sulphide (PbS) nanocrystals were prepared by dissolving anhydrous lead acetate ($Pb(CH_3COO)_2$) in boiling ethanol (C_2H_5OH) and the resulting solution was cooled and then combined with the ethanol solution of sodium sulphide (Na_2S) in ice water. The PbS nanocrystals were formed during hydrolysis and condensation of dissolved species according to the following reaction equation:

$$Pb(CH_3COO)_2 + Na_2S \rightarrow PbS + 2CH_3COO^- + 2Na^+$$
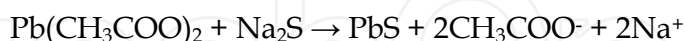
Similarly, ZnO nanocrystals were prepared by dissolving anhydrous zinc acetate ($Zn(CH3COO)_2$) in boiling ethanol and the resulting solution was cooled and then combined with the ethanol solution of sodium hydroxide (NaOH) in ice water. The ZnO nanocrystals were formed during hydrolysis and condensation of dissolved species according to the following reaction equation:

$$Zn(CH_3COO)_2 + 2NaOH \rightarrow ZnO + 2CH_3COO^- + 2Na^+ + H_2O(\uparrow)$$

The unwanted CH_3COO^- and Na^+ impurity ions were removed by centrifuging repeatedly in a mixture of ethanol and heptane. The resulting PbS and ZnO precipitates were either dispersed/suspended in ethanol for mixing with SiO_2 or were dried at 90°C in an oven for characterization.

3.2 Preparation of rare-earths, PbS and ZnO nanocrystals incorporated SiO_2

A silica (SiO_2) sol was prepared by hydrolyzing tetraethylorthosilicate ($Si(OC_2H_5)_4$) or TEOS with a solution of water, ethanol and dilute nitric acid (HNO_3). The mixture was stirred vigorously at room temperature. The SiO_2 was formed during the condensation reaction according to the following equation:

$$Si(OC_2H_5)_4 + 2H_2O \rightarrow SiO_2 + 4C_2H_5OH$$
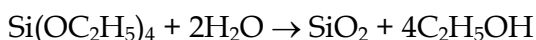
The SiO_2 sol was divided into two parts and one part was mixed with the ethanol suspension of PbS nanocrystals and the other part was mixed with $RE(NO_3) \cdot 6H_2O$ (RE = Ce/Tb/Pr) dissolved in ethanol before adding the ethanol suspension of ZnO nanocrystals and the mixtures were stirred vigorously until thick viscous gels were formed. The gels were dried at room temperature for 3 – 8 days, were ground using a pestle and mortar, and were finally annealed at 600°C in air for 2 hours. Samples that were prepared include SiO_2; $SiO_2:Pr^{3+}/Ce^{3+}/Tb^{3+}$; $SiO_2:Ce^{3+},Tb^{3+}$; $ZnO-SiO_2:Pr^{3+}$; and $SiO_2:PbS$ powders. The molar concentrations of rare-earth ions and ZnO in SiO_2 were varied while that of the PbS nanocrystals was fixed at 0.34 mol%.

4. Results and discussions

4.1 X-ray diffraction

Figure 2 shows the X-ray diffraction patterns of ZnO and PbS nanocrystals. The patterns are consistent with the hexagonal and cubic phases of ZnO and PbS referenced in JCPDS cards number 36-14551 and 05-0592 respectively. The broadening of the diffraction peaks is attributed to smaller particles. The average crystallite sizes estimated from the broadened

XRD peaks were 5 and 6 nm in diameters for ZnO and PbS respectively. Figure 3 shows XRD patterns of SiO_2 and ZnO-SiO_2:Pr^{3+}, all annealed at 600°C for two hours. The concentrations of ZnO and Pr^{3+} in SiO_2 host were 5 and 1 mol% respectively. All the spectra are characterized by the well known broad diffraction of the amorphous SiO_2 peak at $2\theta = \sim$ 20 – 25°. The absence of x-ray diffraction peaks from encapsulated 5 mol% of ZnO nanocrystals and 1 mol% of Pr^{3+} is probably due to their relatively low concentration and/or high scattering background from amorphous SiO_2.
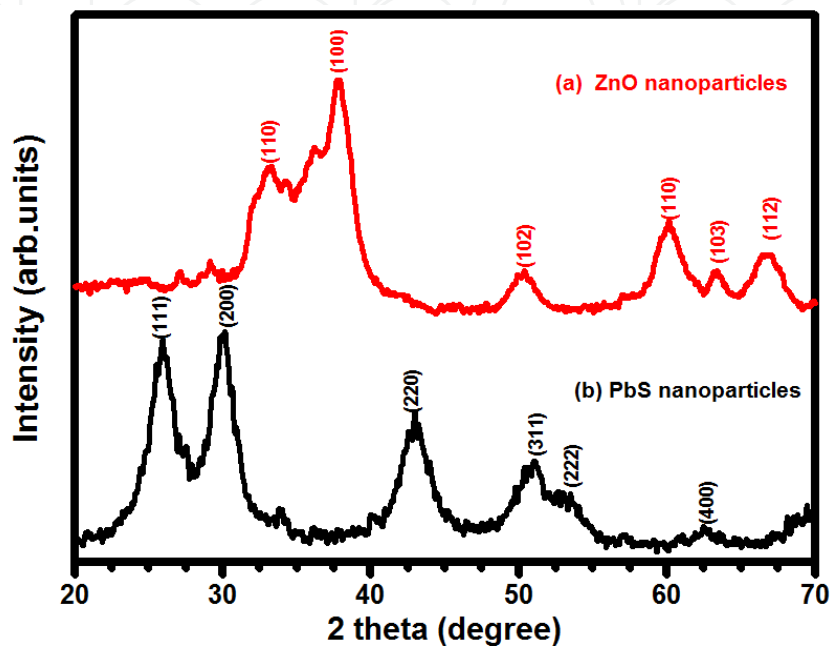
Fig. 2. XRD patterns of (a) ZnO and (b) PbS nanoparticles.
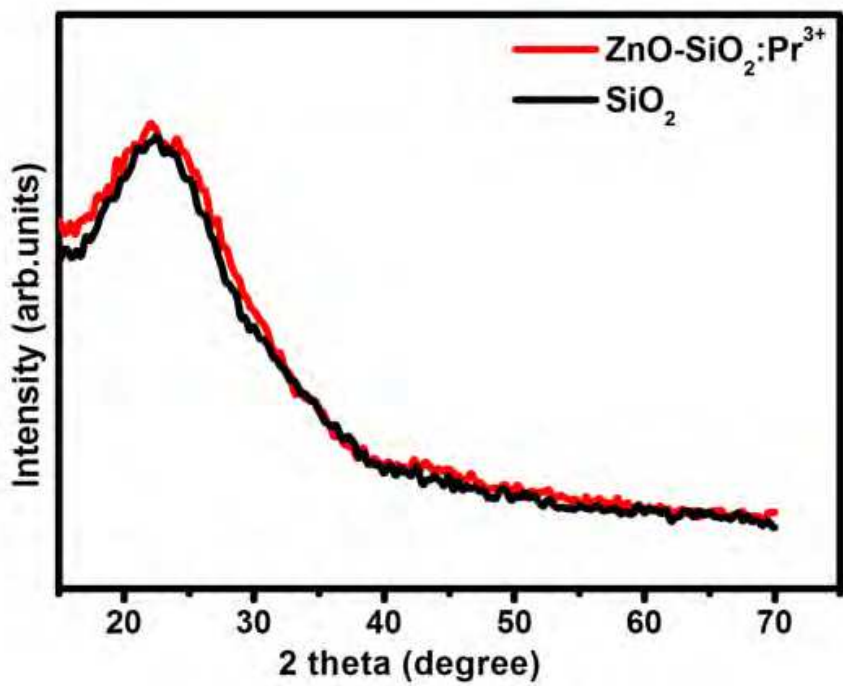
Fig. 3. XRD patterns of SiO_2 and ZnO-SiO_2:Pr^{3+}

4.2 Cathodoluminescence: Properties and intensity degradation

Cathodoluminescence data were recorded using S2000 Ocean Optics CL spectrometer attached to a vacuum chamber of the PHI 549 Auger electron spectrometer (AES) either at base pressure or after backfilling with oxygen gas. Figure 4 presents a simplified schematic diagram of the AES system whose major components are vacuum chamber, housing for the cylindrical mirror analyzer, and electron gun. Attached to the chamber are the fiber optics CL spectrometer and the residual gas analyzer (RGA). The AES and CL spectrometers are connected to two separate computers equipped with programs for recording the Auger and CL data during electron beam irradiation. The Auger and CL data were recorded when the samples were irradiated with a beam of electrons using different accelerating voltages and beam currents.
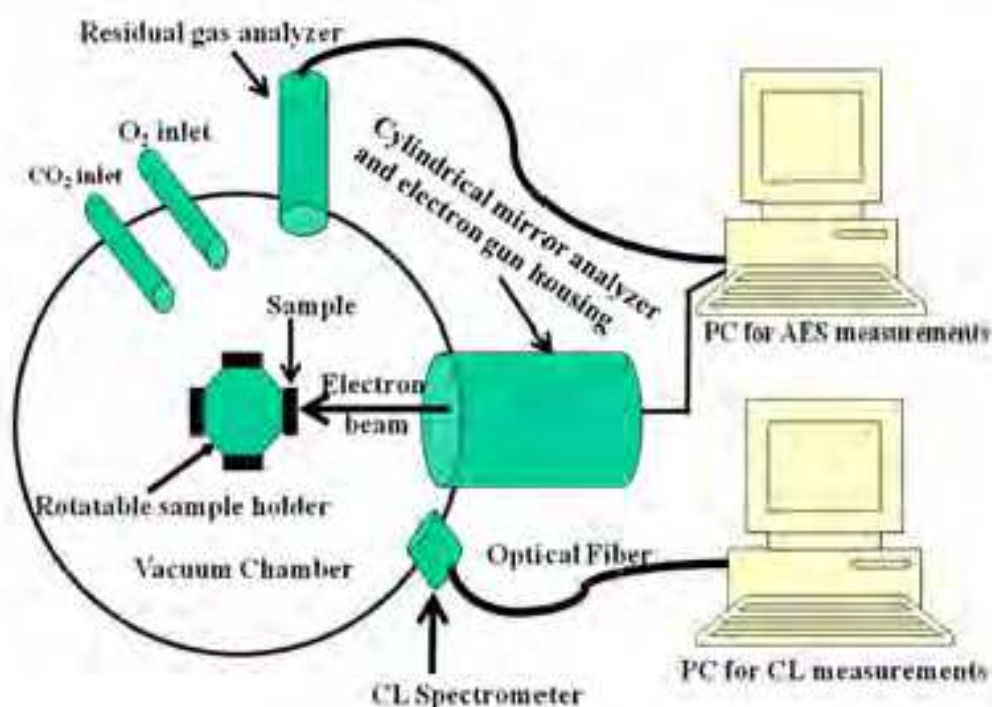
Fig. 4. Schematic diagram of the PHI 549 Auger system.

4.2.1 SiO_2:Ce^{3+},Tb^{3+}

SiO_2:Ce^{3+},Tb^{3+} (Ce^{3+} =Tb^{3+}= 0.5 mol%) powders were irradiated with a 54 mA/cm^2 beam of electrons accelerated at 2 kV in a vacuum chamber of the Auger spectrometer maintained at either 1×10^{-7} or 1×10^{-8} Torr O_2 for 10 hours. Figure 5 compares the normalized CL emission spectra of SiO_2 and SiO_2:Ce^{3+} (0.5 mol%). The inset shows the CL spectrum of SiO_2:Tb^{3+} (0.5 mol%). The SiO_2 spectrum is characterized by a broadband blue emission with a maximum at 445 nm and a satellite peak at 490 nm. The visible emission from SiO_2 is attributed to carrier trapping by structural defects (Lin and Baerner., 2000; Han et al., 2002; Gu et al., 1999) or charge transfer between Si and O atoms (García et al., 1995). Upon incorporation of Ce^{3+} and Tb^{3+} the defects emission at 445 nm from SiO_2 was suppressed and blue and green emissions from Ce^{3+} and Tb^{3+} were observed. The blue emission with a maximum at 489 nm can be attributed to 4f→5d transitions of Ce^{3+} while the line emissions with the main

emission at ~550 nm in the inset can be attributed to the 5D→ 7F transitions of Tb^{3+}. Figure 6 shows the CL emission spectra of the co-activated SiO$_2$:Ce^{3+},Tb^{3+} before and after electron irradiation. The insets are the photographs of the irradiated area in the beginning and at the end of irradiation. The emission peaks are associated with radiative transitions of Tb^{3+} ions. The main emission peak was observed at ~550 nm and it is associated with $^5D_4 \rightarrow {}^7F_5$ transitions of the Tb^{3+} ions. The emission intensity of this peak was reduced by ~50% after 10 hours of irradiation as shown by the fading of green luminescence in the inset. The synergies between the CL intensity degradation and the changes in the surface chemistry were determined using the Auger electron and the X-ray photoelectron spectroscopy.
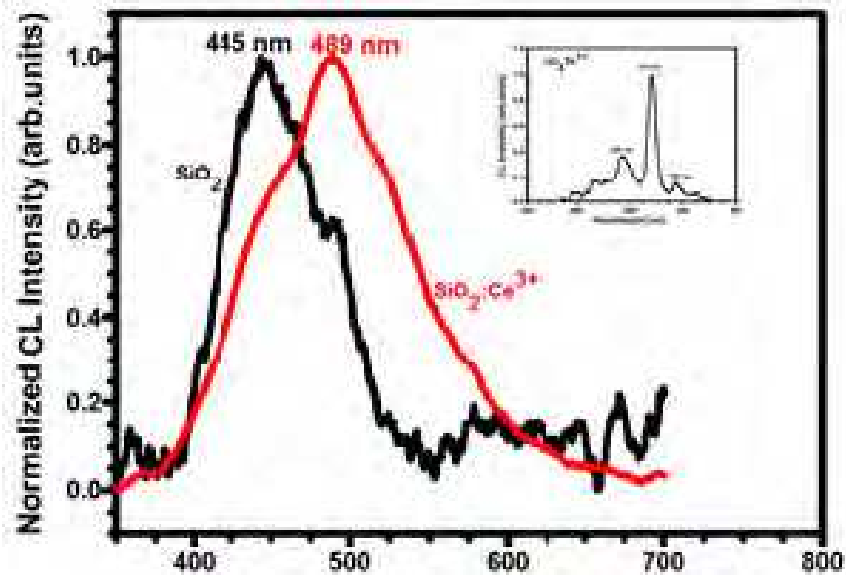
Fig. 5. Normalized CL intensity of SiO$_2$ and SiO$_2$:Ce^{3+}. The inset is the CL intensity versus wavelength spectrum of SiO$_2$:Tb^{3+}.
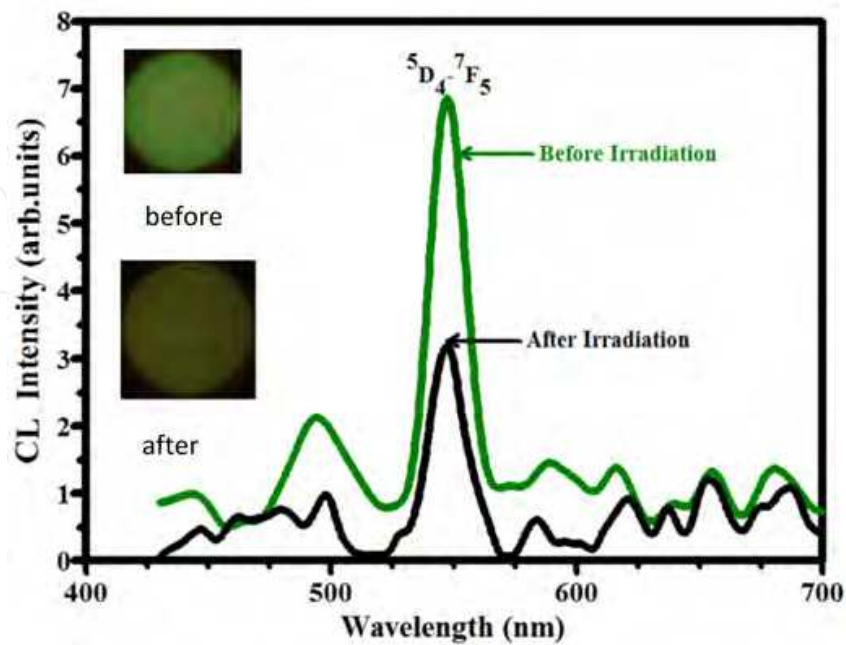

Fig. 6. CL intensity spectra of SiO$_2$:Ce^{3+},Tb^{3+} before and after electron irradiation.

Figure 7 shows the Auger spectra of the SiO_2 powder before and after electron irradiation. The main features in both spectra are the Si (76.9 eV) and O (505 eV) peaks. Note the decrease in the O Auger peak intensity after 10 hours of continuous irradiation. The Auger peak at 76.9 eV is associated with Si in SiO_2. As a result of the prolonged electron irradiation this peak shifted to 82.7 eV and its intensity was reduced slightly. Thomas (Thomas; 1974) attributed the shift to change in the density of state in the valence band rather than the shift in the binding energies of Si. The XPS data showed that with continuous irradiation an Auger peak associated with elemental Si developed at 98.2 eV and there was also a subsequent change in colour of the chathodoluminescence at the irradiated area.

Figure 8 shows the decrease/degradation of the CL intensity and the Auger-peak-to-peak-heights (APPHs) of oxygen (O), silicon (Si) and adventitious carbon (C) as a function of electron dose for the data recorded when the chamber was maintained at 1×10^{-7} Torr O_2. During electron irradiation, the decrease in the CL intensity was simultaneous with rapid desorption of oxygen from the surface as shown in the figure. Ce^{3+} and Tb^{3+} ions were not detected probably due to their relatively low concentration. While the C peak was almost unchanged, the Si peak was shown to decrease marginally but steadily. Similar trend was observed when the chamber pressure was 1×10^{-8} Torr O_2.
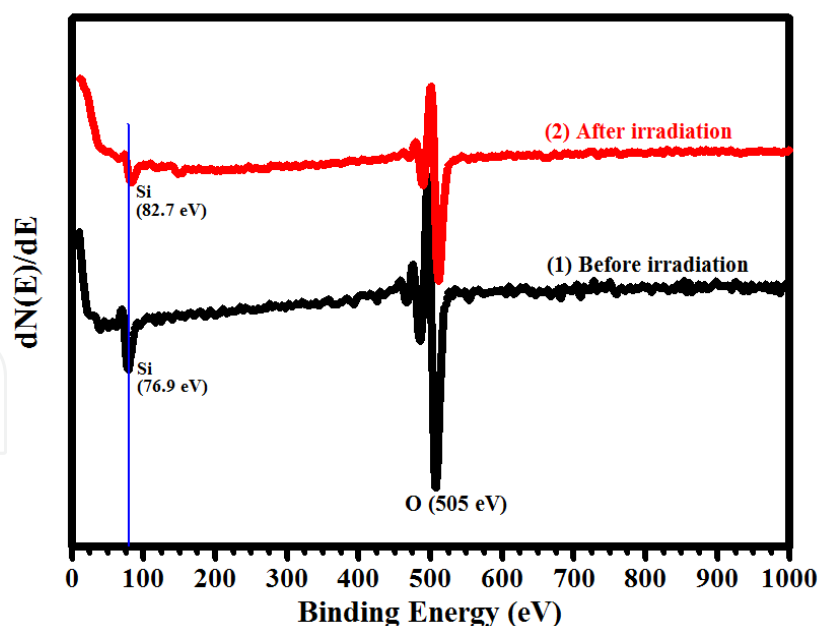

Fig. 7. AES spectra of SiO_2:Ce^{3+},Tb^{3+} before and after electron irradiation.
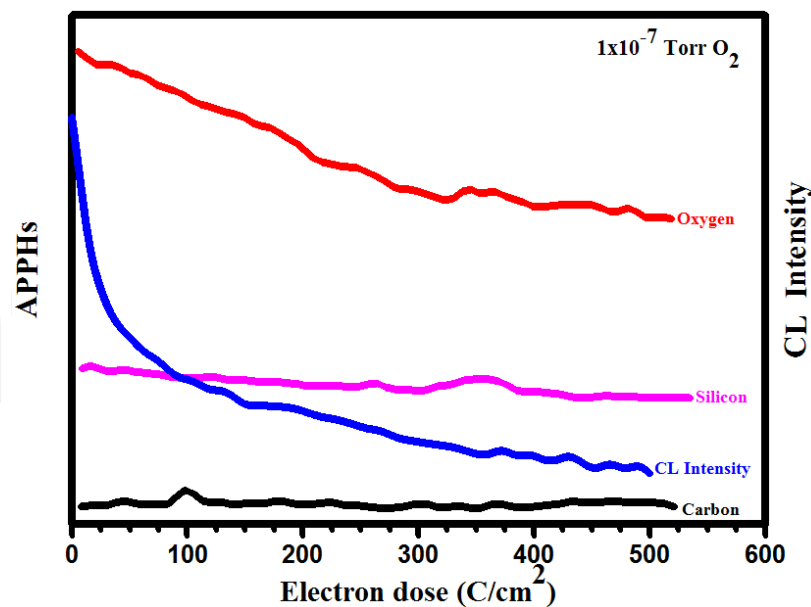
Fig. 8. Auger peak-to-peak-heights of O, Si, C; and the CL intensity as a function of electron dose (Ntwaeaborwa et al., 2006).

Figure 9 and 10 compare respectively the normalized O APPHs and the CL intensity degradation as functions of electron dose at the chamber pressures of 1×10^{-7} and 1×10^{-8} Torr O_2. As shown in figure 9, the rate of O desorption was faster at the low flux (10^{-8} Torr O_2) of O_2 while that of the CL intensity degradation in figure 10 was faster at higher oxygen pressure (10^{-7} Torr O_2). The data in figure 9 and 10 suggest that there is a correlation between O desorption and the CL intensity degradation.
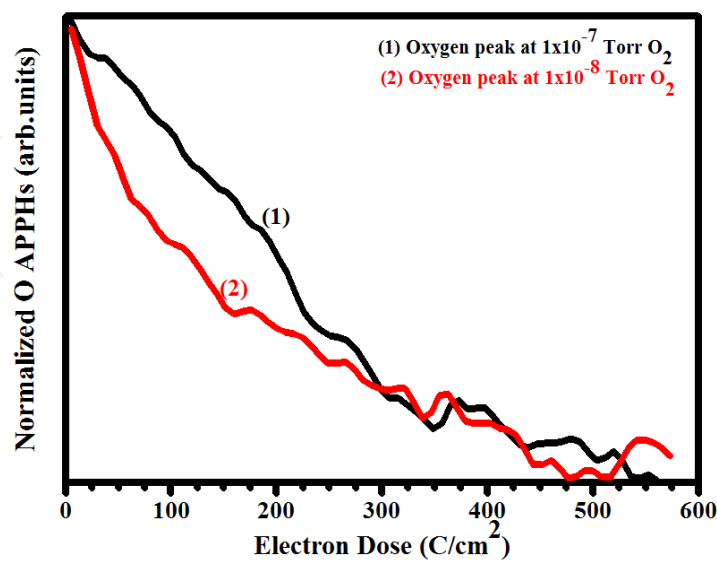
Fig. 9. Normalized O APPHs as a function of electron dose at 1×10^{-7} and 1×10^{-8} Torr O_2 (Ntwaeaborwa et al., 2007).
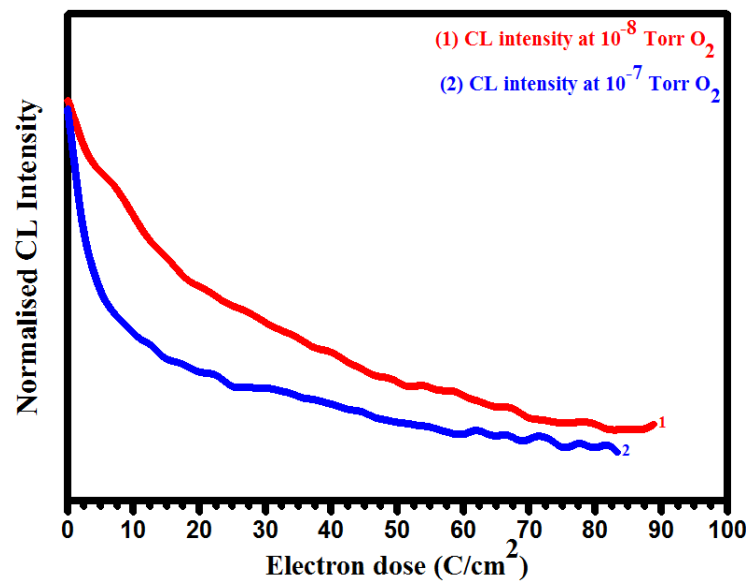
Fig. 10. Normalized CL intensity as a function of electron dose at 1×10⁻⁷ and 1×10⁻⁸ Torr O₂ (Ntwaeaborwa et al., 2006).

X-ray photoelectron spectroscopy (XPS) was used to investigate the correlation between the CL intensity degradation and the changes on the surface chemistry. The XPS data were recorded from the $SiO_2:Tb^{3+},Ce^{3+}$ powders before and after electron irradiated. Figure 11 compares the high resolution Si 2p XPS peaks before and after irradiation. Note the shift of 0.2 eV to the right in the peak position, development of the new peak at 98.2 eV and the narrowing of the spectrum after electron irradiation. While the peak shift and narrowing can be attributed to surface charging, among other things, the development of the new peak can be attributed to the chemical changes that occurred on the surface during irradiation.
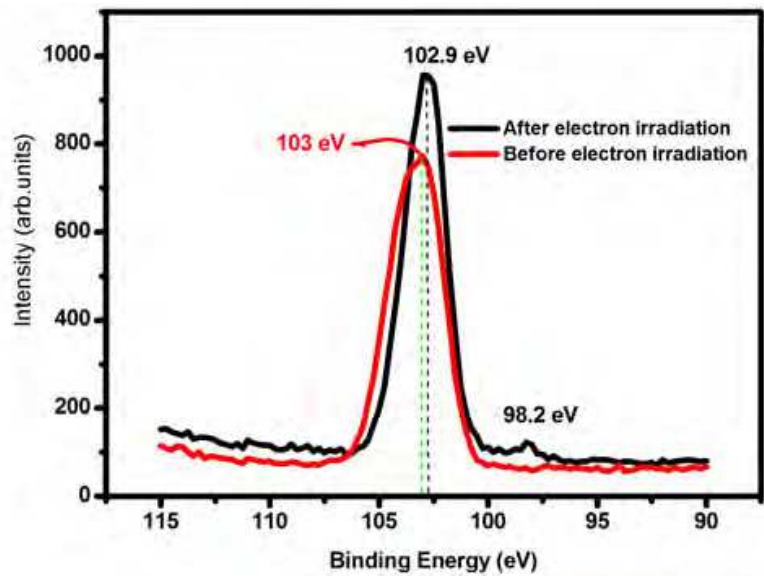

Fig. 11. High resolution Si XPS peaks before and after electron irradiation.

Figures 12 and 13 show respectively the fitted high resolution Si 2p XPS peaks before and after irradiation. The peaks at 102.5, 103.7 and 104.8 eV in figure 12 can be assigned to SiO_x

(x < 2), SiO_2 and chemisorbed species (from atmospheric oxygen/moisture) respectively (Nagpure et al.; 2011). Note the absence of the peak from chemisorbed species and the appearance of two additional peaks at 100.6 eV and 98.2 eV in figure 12 that can be assigned to SiC (Nagpure et al.; 2011) and elemental Si (Moulder et al.; 1992) respectively. The well known effect of the prolonged electron beam irradiation of SiO_2 is the breaking (dissociation) of Si-O bond and the subsequent desorption of oxygen. As shown in the XPS spectrum after electron beam irradiation in figure 11, the depletion of oxygen was accompanied by a growth of free (elemental) silicon (Si) at 98.2 eV. As a result of oxygen desorption the surface was rich in Si and the remaining structure was probably an oxygen deficient SiO_x (0<x<2). The mechanism of desorption of oxygen from SiO_2 is beyond the scope of this chapter and the readers are referred to the literature cited for further reading (Carriere and Lang, 1977; Knotek and Feibelman, 1978; Thomas, 1974; Fiori and Devine, 1984). It is most likely that the oxygen deficient SiO_x was non-luminescent and it therefore contributed to the CL intensity degradation (Ntwaeaborwa et al., 2006, 2007).
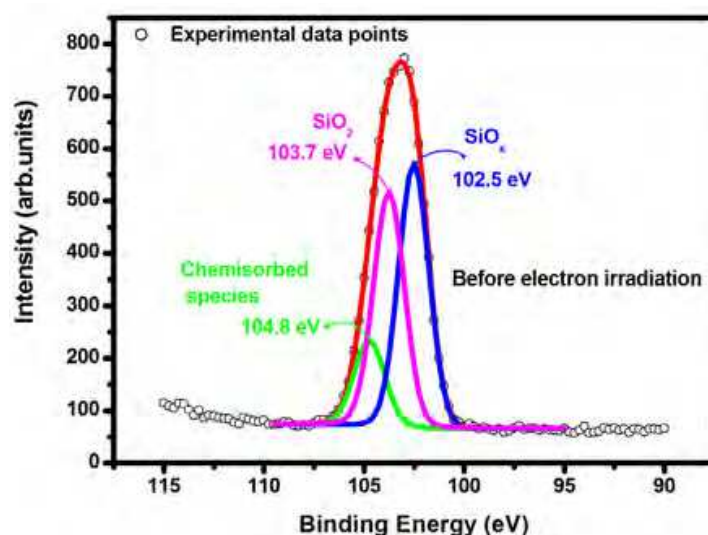

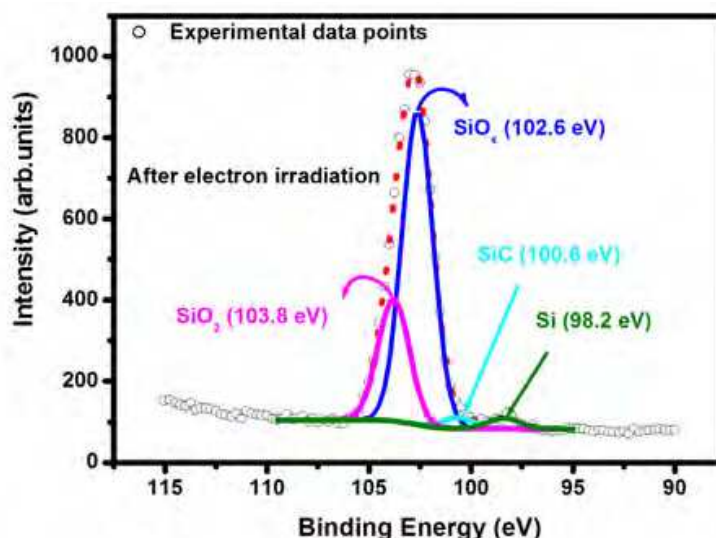Fig. 12. Fitted high resolution Si 2p XPS peak before electron irradiation.

Fig. 13. Fitted high resolution Si 2p XPS peak after electron irradiation.

4.2.2 ZnO-SiO$_2$:Pr^{3+} and SiO$_2$:Ce^{3+},Pr^{3+}

In this section the effects of ZnO nanoparticle, Ce^{3+} and Pr^{3+} concentrations on cathodoluminescence intensities of ZnO-SiO$_2$:Pr^{3+} and SiO$_2$:Ce^{3+},Pr^{3+} are discussed. Figure 14 shows the CL spectra of SiO$_2$:Pr^{3+}, with different concentrations (0.05 – 0.25 mol%) of Pr^{3+}, measured in the AES vacuum chamber at a base pressure of 10^{-8} Torr. Note that relatively low concentrations of Pr^{3+} were used to avoid quenching at higher concentrations. The CL intensity increased with concentration from 0.05 to 0.2 mol% and it decreased when the concentration was increased to 0.25 mol% due to concentration quenching effect. It is well known that at higher concentrations of light emitting ions, luminescence can be quenched as a result of clustering of or cross relaxation between the ions (Blasse and Grabmaier, 1994; Solé et al., 2005). The CL emission spectra are characterized by multiple line emissions in the visible region of the electromagnetic spectrum. The main emission associated with $^3P_0 \rightarrow ^3H_6$ transitions of Pr^{3+} was observed at 616 nm and minor emissions due to transitions from $^3P_0$ and $^1D_2$ to $^3H_{(J = 6, 5, 4)}$ and $^3F_{(J = 2, 3, 4)}$ were also observed. These transitions were not measured but were assigned according to the literature cited (Mhlongo et al., 2011a, Sokólska et al., 2000). The inset of figure 13 shows the maximum CL intensity of the 616 nm peak as a function of Pr^{3+} concentration illustrating the increase in intensity with concentration from 0.05 to 0.2 mol% and a sudden decrease when the concentration was increased to 0.25 mol%.
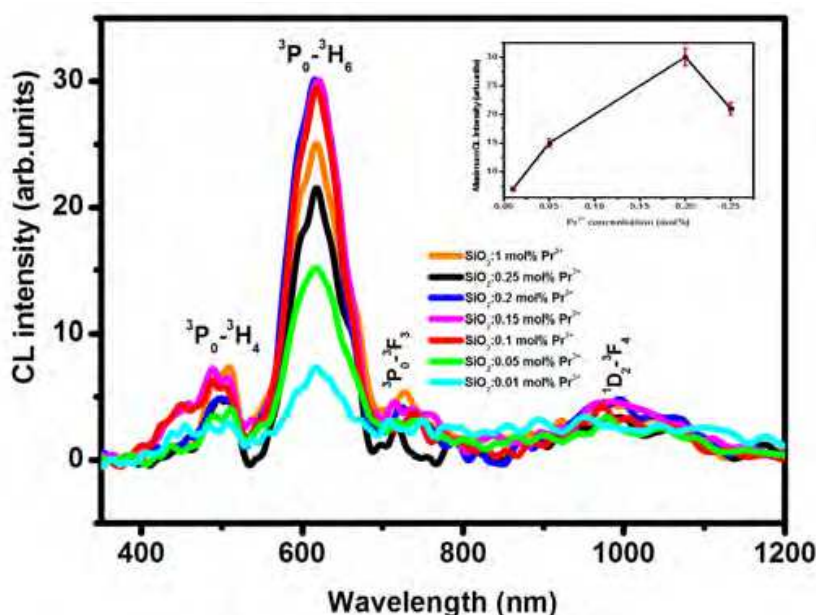

Fig. 14. CL spectra of SiO$_2$:Pr^{3+} with different concentrations of Pr^{3+}.

Figure 15 compares the CL emission spectra of SiO$_2$, SiO$_2$:1mol%Pr^{3+} and ZnO-SiO$_2$:1mol%Pr^{3+} (ZnO = 5mol%) powders recorded when the powders were irradiated with a beam of 2 keV electrons and a beam current of 20 µA in the chamber kept at a base pressure of 1.6×10^{-8} Torr. With incorporation of Pr^{3+}, the blue emission of SiO$_2$ at 445 nm was suppressed and all the observed emissions were due to transitions in Pr^{3+}. The main emission at 616 nm was enhanced considerably by the incorporation of ZnO nanopareticles. This emission is 2× more intense than the emission from SiO$_2$:Pr^{3+} suggesting that ZnO contributed to this enhancement by transferring excitation energy to Pr^{3+} ions. Note that

because of severe charging upon irradiation with electrons, cathodoluminescence of ZnO nanoparticles could not be measured. However it is a well known phenomenon that ZnO nanoparticles display dual emission in the UV and visible region irrespective of the type of excitation (i.e. UV photons or electrons) (Mhlongo et al., 2011b). Since both the UV and defects emissions were not detected when ZnO nanoparticles were incorporated in SiO$_2$:Pr^{3+} and there was a subsequent increase in the red emission from Pr^{3+}, it is reasonable to attribute the increase to energy transfer from ZnO to Pr^{3+}. The reader is referred to the literature cited to read about the mechanism of energy transfer from ZnO to rare-earth ions in glassy SiO$_2$ host (Bang et al., 2006; Ntwaeaborwa and Holloway, 2005; Mhlongo et al., 2010)

Figure 16 shows the CL emission spectra of Ce^{3+}-Pr^{3+} co-activated SiO$_2$ phosphors. The concentration of Pr^{3+} was fixed at 0.2 mol% while that of Ce^{3+} was varied from 0.2 – 2 mol%. The spectra were recorded when the powders were irradiated with 2 keV electrons and a beam current of 8.5 µA in the AES vacuum chamber maintained at a base pressure of 1.2 ×10^{-8} Torr. The CL spectrum of Pr^{3+} singly doped SiO$_2$ consists of a major emission peak at 616 nm and minor peaks at 510 and 489. The CL spectrum of Ce^{3+} consists of broad emission peak with a maximum at 489 nm. Notice the suppression of the Pr^{3+} emission in co-activated SiO$_2$:Ce^{3+},Pr^{3+} and the change in PL intensity of the 489 nm peak with Ce^{3+} concentration. The maximum intensity was observed when 1 mol% of Ce^{3+} was co-doped with 0.2 mol% of Pr^{3+} as shown in the inset of figure 16. The intensity was quenched, probably as a result of concentration quenching effects, when the Ce^{3+} was increased to 1.5 and 0.2 mol%.
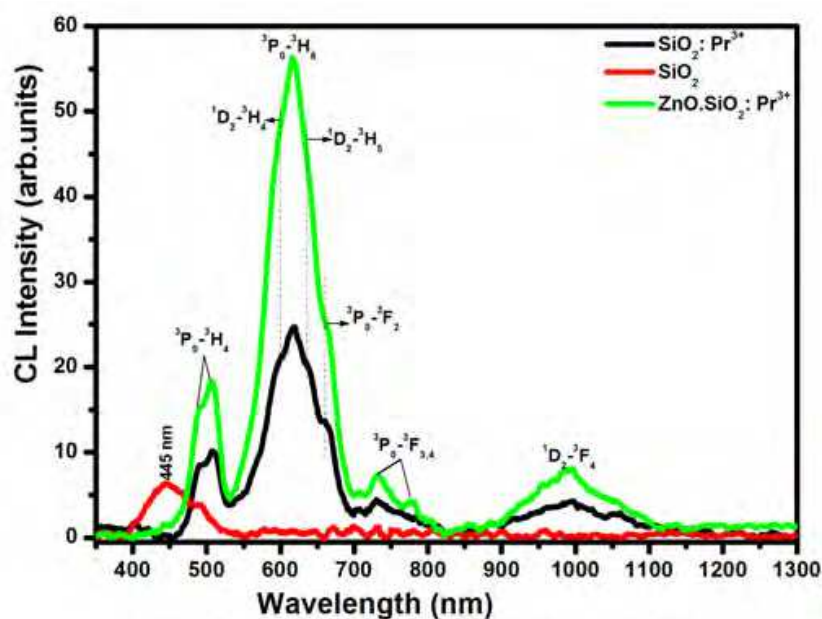

Fig. 15. CL spectra of SiO$_2$, SiO$_2$:Pr^{3+} and ZnO-SiO$_2$:Pr^{3+} (Mhlongo et al., 2010)

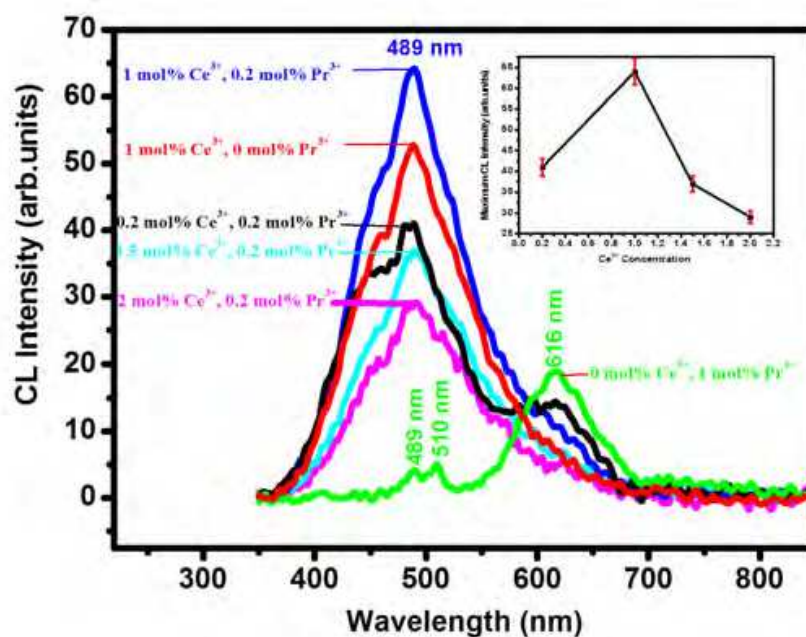Fig. 16. CL spectra of SiO_2:Ce^{3+}, SiO_2:Ce^{3+},Pr^{3+} and SiO_2:Pr^{3+}. The inset is the maximum CL intensity of the 489 peak as a function of Ce^{3+} concentration.

The fact that the increase in the blue emission at 489 nm was simultaneous with the quenching of Pr^{3+} emission from SiO_2:Ce^{3+},Pr^{3+} (Ce^{3+} = 1 mol% and Pr^{3+} = 0.2 mol%) suggests that energy was transferred from Pr^{3+} to Ce^{3+}. Note that the energy associated with the $^1P_0 \rightarrow {}^3H_6$ transition of Pr^{3+} is 2.0 eV (616 nm), which is too low to transfer to Ce^{3+} at 2.5 eV (489 nm). On the other hand, the energy associated with the $^3P_0 \rightarrow {}^3H_4$ transition of Pr^{3+} occurs at the same energy position of 2.0 eV (489 nm) as the blue emission from Ce^{3+}. It is therefore reasonable to speculate that energy was transferred resonantly or by phonon mediated processes from the $^3P_0$ state of Pr^{3+} to $5d^1$ states of Ce^{3+}. Before discussing the proposed mechanism of energy transfer, it is important to discuss briefly the transitions responsible for blue emission in Ce^{3+}. Shown in figure 17 is the deconvoluted CL emission spectrum of SiO_2:Ce^{3+},Pr^{3+} (Ce^{3+} = 1 mol%) recorded during irradiation with 2 keV beam of electrons and a beam current of 8.5 µA at a base pressure of 1.2 ×10^{-8} Torr. The 489 nm peak is deconvoluted into two Gaussian peaks, one at 480 nm and the other one at 525 nm. The 4f ground state of the Ce^{3+} is split into two components ($^2F_{5/2}$ and $^2F_{7/2}$) due to spin-orbit interaction while the excited $5d^1$ state can be split into 2-5 components by the crystal field (Ntwaeaborwa et al., 2008; Mhlongo et al., 2011a). Here we consider a case where the $5d^1$ is split into two components, namely the upper $^2D_{5/2}$ and the lower $^2D_{3/2}$. We speculate that the absorbed excitation energy causes transition from the ground state to the upper $^2D_{5/2}$ state followed by radiationless transition to the lower $^2D_{3/2}$ and a subsequent radiative transition to the $^2F_{7/2}$ (480 nm) and $^2F_{5/2}$ (525 nm) energy states.
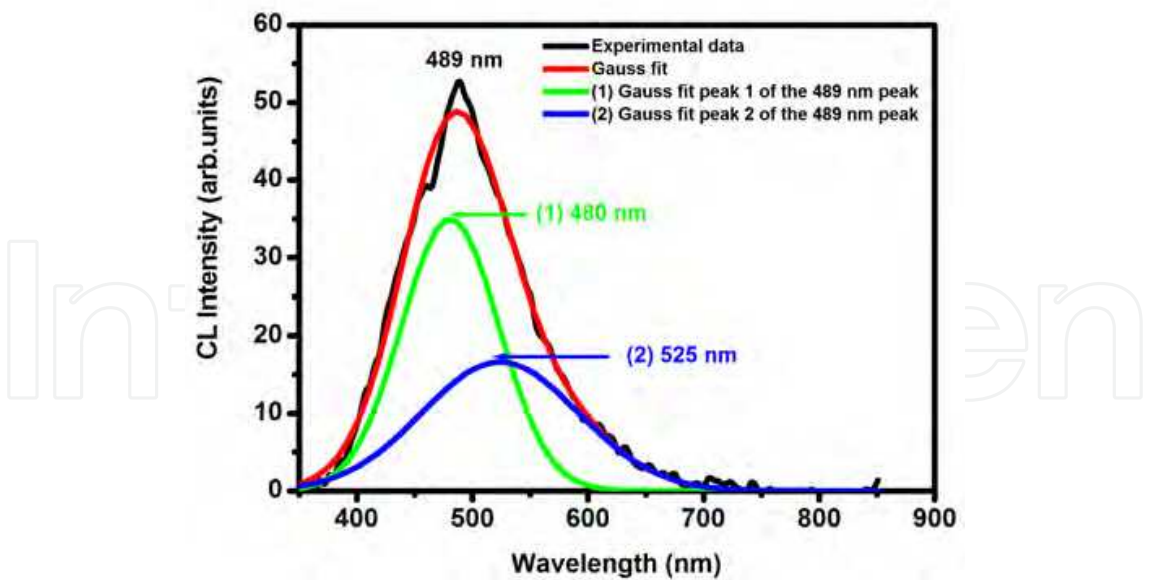
Fig. 17. Deconvoluted CL emission spectrum of SiO$_2$:Ce^{3+}.

The proposed mechanism of energy transfer from Pr^{3+} to Ce^{3+} is presented in figure 18. According to this mechanism, the absorbed excitation energy causes transition from the ground state (^{3}H$_4$) to higher energy states (4f5d) of Pr^{3+}. This is followed by a radiationless transition to the ^{3}P$_{2,1,0}$ states of Pr^{3+}. In a Pr^{3+} singly doped SiO$_2$ the ^{3}P$_{1,0}$ states will be followed by radiative transitions to the ^{3}H$_{6,5,4}$ states. However, in the Ce^{3+}-Pr^{3+} co-activated SiO$_2$ the ^{3}P$_0$ state of Pr^{3+} will transfer energy resonantly or by phonon-assisted processes to the 5d^1 states of Ce^{3+} resulting in an enhanced blue emission during radiative transition to the ground state. This is only possible if the transfer rate is faster than the radiative transition to the ^{3}H$_{6,5,4}$ states. Similar mechanism was reported by Ntwaeaborwa et al. (Ntwaeaborwa et al., 2008) for energy transfer between Eu^{3+} and Ce^{3+}.
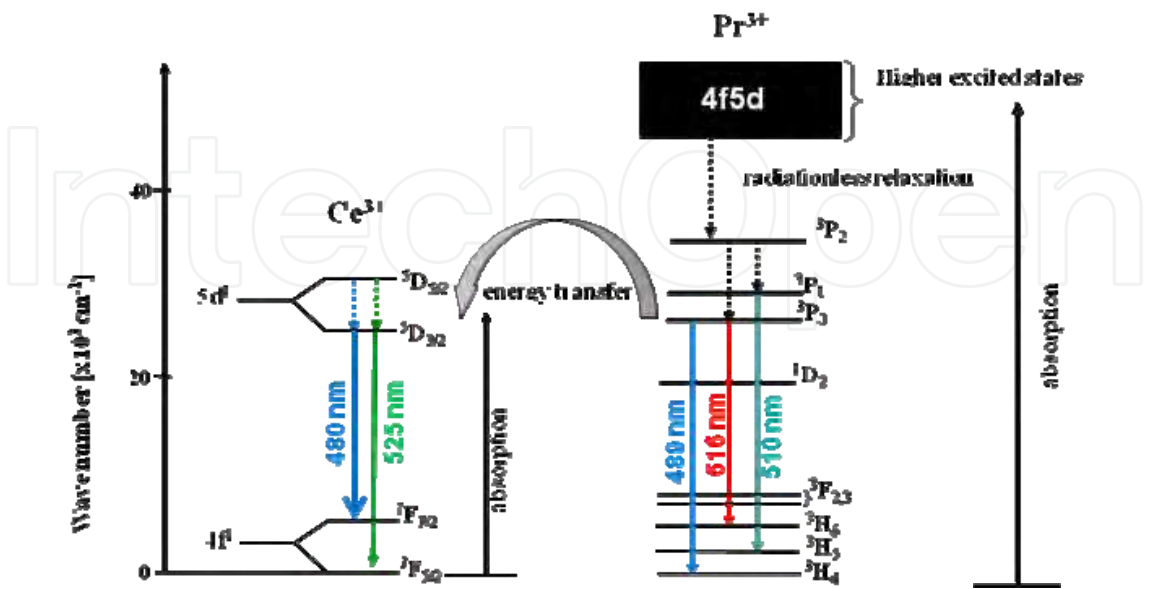

Fig. 18. Simplified energy level diagrams of Ce^{3+} and Pr^{3+} illustrating energy transfer from Pr^{3+} to Ce^{3+}.

The effect of accelerating voltage on the brightness of SiO_2:Ce^{3+},Pr^{3+} (Ce^{3+} = 1 mol% and Pr^{3+}=0.2 mol%) was evaluated by varying the voltage from 1 – 5 kV when the beam current was fixed at 8.5 μA. Figure 19 shows the CL intensity as a function of accelerating voltage. As shown in the inset, the CL intensity of the 489 nm peak is increasing linearly with voltage from 1 to 5 kV. It is well known that the depth of penetration by incident electrons is proportional to the accelerating voltage (Kumar et al., 2010), i.e. high the accelerating voltage deeper will be the penetration. The proportional increase in the CL intensity (brightness) with accelerating voltage suggests that the rate of generation of free electron and holes was high at greater penetration depths and a subsequent increase of radiative recombination. A lack of luminescence saturation at voltages up to 5 kV is a sign of good prospect for this phosphor to be used in low voltage (1 – 10kV) field emission display technology.
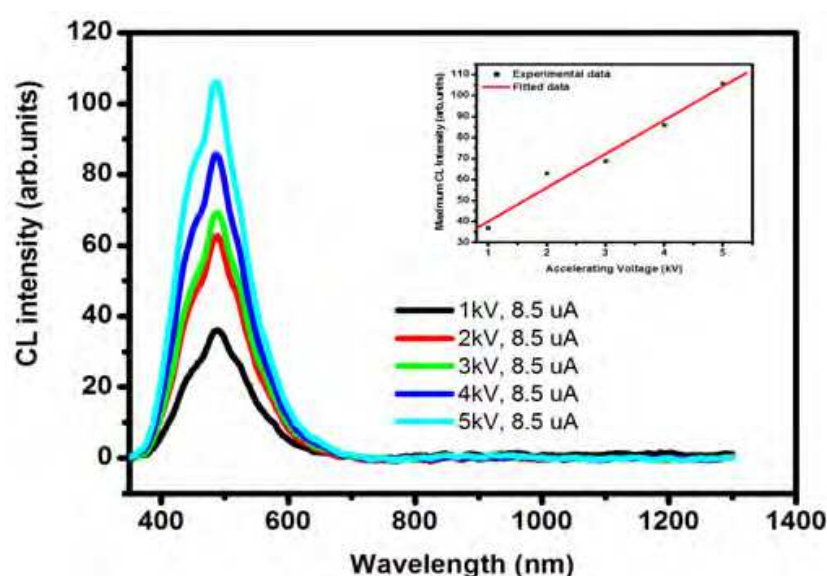

Fig. 19. The effect of accelerating voltage on the CL intensity of SiO_2:Ce^{3+},Pr^{3+}.

4.2.3 SiO₂:PbS

In this section, cathodoluminescent properties and intensity degradation of SiO_2:PbS phosphor are discussed. The preparation of the samples was discussed in section 1.2. The concentration of PbS nanoparticles in SiO_2 was 0.34 mol%. The CL data were recorded when the SiO_2:PbS powders were irradiated with a 2 keV beam of electrons in the Auger spectrometer chamber at different oxygen pressures. The Auger-peak-to-peak-heights (APPHS) of O, Si and C and CL intensity as a function of electron dose resembled that of SiO_2:Ce^{3+},Tb^{3+} in figure 8 suggesting that the decrease in the CL intensity was simultaneous with desorption of O. Figure 20 shows broadband CL emission spectra, before and after electron irradiation, with a maximum at ~700 nm. While the CL emission from pure SiO_2 was observed at 445 nm (figure 5), the CL emission from pure PbS nanoparticles could not be recorded due to excessive surface charging. It is however well known that light emission from PbS nanoparticles associated with excitonic recombination is usually in the near infrared region at 1100 – 1700 nm (Ntwaeaborwa et al., 2009a, which is blue-shifted from PbS bulk emission at ~3000 nm due to quantum confinement effects. Therefore the orange-red emission in figure 20 is neither coming from SiO_2 nor PbS nanoparticles. This emission

is similar to emission associated with transitions in Pb^{2+} ions in ZnS:Pb^{2+} (Bol and Meijerink, 2001) and SiO_2:Pb^{2+} (Ntwaeaborwa et al., 2009b). Although the exact mechamism of this emission is not known yet, it is reasonable to attribute the emission to transisions in Pb^{2+}. This can only be possible if Pb^{2+} ions are selectively excited. Note that blue, green and red emissions from Pb^{2+} have been reported and the red emission, similar to the one in figure 20, was attributed to $^3P_{0,1} \rightarrow {}^1S_0$ transition of Pb^{2+} (Bol and Meijerink, 2001). As shown in the inset of figure 20, the red-orange cathodoluminescence degraded by more than 50% following the prolonged irradiation by 2 keV electrons. Similar mechanism that involves desorption of O and a subsequent formation of less luminescent SiO_x (x < 2) discussed in section 2.2.1 can be used to explain the CL intensity degradation of the SiO_2:PbS phosphor.
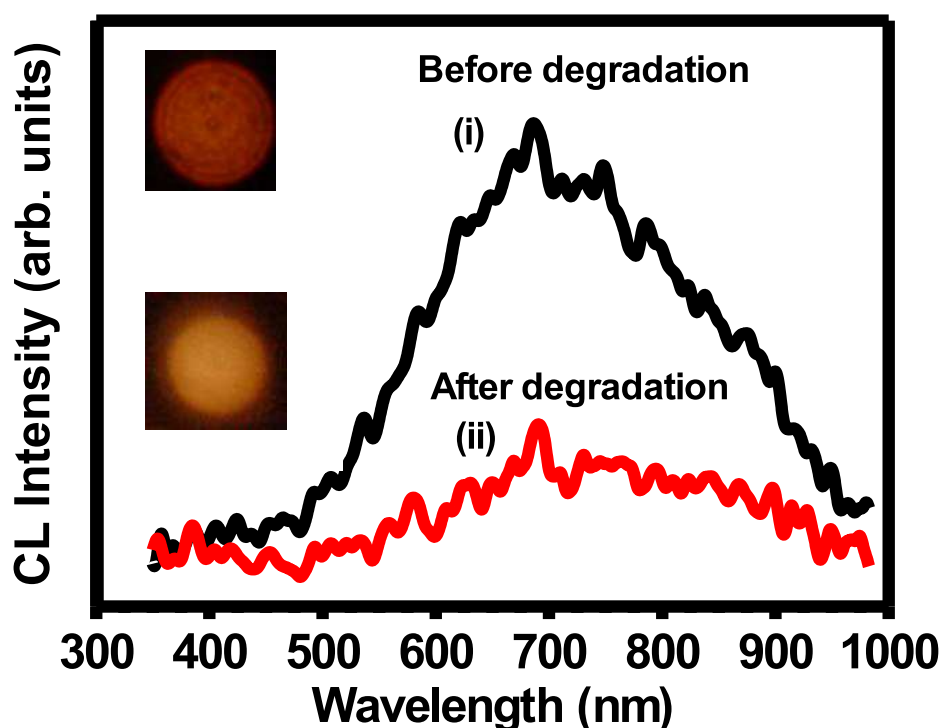

Fig. 20. CL emission spectra of SiO_2:PbS before and after electron irradiation.

5. Conclusion

Green, blue and orange-red cathodoluminescence was observed, respectively, from SiO_2:Ce^{3+},Tb^{3+}; SiO_2:Ce^{3+},Pr^{3+} and SiO_2:PbS phosphors prepared by the sol-gel method. Green emission from Tb^{3+} was enhanced by Ce^{3+} co-doping. The CL intensity of the green emission degraded by 50% when irradiated with a beam of electrons for 10 hours and the CL intensity degradation was simultaneous with desorption of O from the surface. The degradation was attributed to the formation of oxygen deficient SiO_2 (x<2) layer. Enhanced blue emission from Ce^{3+} was observed from Ce^{3+}-Pr^{3+} co-doping while the red emission of Pr^{3+} suppressed. Possible mechanism of energy transfer from Pr^{3+} to Ce^{3+} was discussed. Orange-red cathodoluminescence from SiO_2:PbS was attributed to $^3P_{0,1} \rightarrow {}^1S_0$ transition of Pb^{2+}. SiO_2 is a potential host matrix for rare-earths and semiconducting nanocrystals for preparation of phosphors that can be used in light emitting devices including cathode ray tubes and field emission displays.

6. Acknowledgment

7. References

[1] Nogami, M., Enomoto, T., Hayakawa, T. (2002). Enhanced fluorescence of Eu^{2+} induced by energy transfer from nanosized SnO_2 crystals in glass. *J. Lumin.* Vol. 97, No. 3-4, pp. (147-152)

[2] Ntwaeaborwa, O.M., Swart, H.C., Kroon, R.E., Botha, J.R., Holloway, P.H. (2007). Cathodoluminescence degradation of SiO_2:Ce,Tb powder phosphors prepared by a sol-gel process. *J. Vac. Sci. Technol. A.* Vol. 25, No. 4, pp. (1152-1155).

[3] Ntwaeaborwa, O.M., Swart, H.C., Kroon, R.E., Botha, J.R., Ngaruiya, J.M., Holloway, P.H. (2008). Enhanced photoluminescence of rare-earth activators in sol-gel derived SiO_2 by energy transfer from ZnO nanoparticles and co-activators, In: *Photoluminescence Research Progress*, Wright H.K. and Edwards, G.V., pp. (287-306), Nova publishers, 978-1-60456-538-6, New York.

[4] Hench, L.L., Wesk, J.K. (1990). The Sol-Gel Proces, *Chem. Rev.*, Vol. 90, No. 1, pp. (33-72).

[5] Ding, J.Y., Day, D.E. (1991). Preparation of silica glass microsphere by sol-gel, *J. Mat. Res*, Vol. 6, No. 1, pp. (168-174).

[6] Ntwaeaborwa, O.M.; Swart H.C.; Kroon, R.E.; Holloway P.H.; Botha, J.R. (2006), Enhanced luminescence and degradation of SiO_2:Ce^{3+},Tb^{3+} powder phosphor prepared by a sol-gel process, *J. Phys. Chem. Sol.*, Vol. 67, pp (1749-1753)

[7] Reisfeld, R., Gaft M., Saridarov, T., Panczer, G., Zelner, M. (2000). Nanoparticles of cadmium sulfidewith europium and terbium in zirconia films having intensified luminescence, *Mat. Lett,* Vol. 45, No. 3, pp. (154-156).

[8] Holloway, P.H., Sebastian, J., Trottier, T., Jones, S., Swart, H., Petersen, R.O. Degradation mechanisms and vacuum requirements for FED phosphors. (1996). *Mat. Res. Soc. Symp. Proc*, Vol. 424, pp. (425-431).

[9] Holloway, P.H., Trottier, T.A., Sebastian, S., Jones, S., Zhang, X.-M., Bang, J.-S., Abrams, B., Thomes, W.J., Kim, T.J. (2000). Degradation of field emission display phosphors, *J. Appl. Phys.*, 88(1), pp. (483-488)

[10] Knotek, M.L. and Feibelman, P.J. (1978). Ion desorption by core-hole Auger decay, *Phys. Rev. Lett.*, Vol. 40, No. 14, pp. (964-967)

[11] Stoffers, C.; Yang, S.; Jacobsen, S. M. and Summers, C.J. (1996). Saturation of phosphor under low voltage excitation, *J. Soc. Inf. Display.* Vol. 4, No. 4, pp. (337-341)

[12] Raue, R.; Vink, A.T. and Welker T. (1989). Phosphors screens in cathode ray tubes for projection television *Phillips Tech. Rev*, Vol. 44, No. (11-12), pp. (335 – 347).

[13] Swart, H.C.; Oosthuizen, L.; Holloway, P.H. & Berning G.L.P. (1998). Degradation behavior of ZnS phosphors under different experiment conditions, *Surf. Interface Anal.*, Vol. 26, No. 5, pp (337-342)

[14] Itoh, S.; Kimizuka, T. and Tonegwa T. (1989). Degradation mechanism for low voltage cathodoluminescence sulphide phosphors, *J. Electrochem. Soc.*, Vol. 136, No. 1819-1823

[15] Klein, L.C. (1985). Sol-gel processing of silicates, *Ann. Rev. Mater. Sci.*, 15, pp. (227-248)

[16] Huang, H-H.; Orler, B. and Wilkes, G.L. (1985). Ceramers: Hybrid materials incorporating polymeric/oligomeric species with inorganic glasses by a sol-gel process – 2. Effect of acid content on the final product, *Polymer Bulletin.*, Vol. 14, No. , pp. (557-564)

[17] Nagpure, I.M.; Pitale, S.S.; Tshabalala, K.G.; Kumar, V.; Ntwaeaborwa, O.M., Terblans, J.J. and Swart, H.C. (2011). Luminescence response and CL degradation of combustion synthesized spherical SiO$_2$:Ce nanophosphor, *Mater. Res. Bull.*, doi:10.1016/j.materresbulls.2011.08.051

[18] Thomas, S. (1973). Electron-irradiation effect in the Auger analysis of SiO$_2$, *J. Appl. Phys.*, Vol. 45, No. 1, pp (161-166).

[19] Lin, J. and Baerner K. (2000). Tunable photoluminescence in sol-gel derived silica xerogels, *Mat. Lett.*, Vol. 46, No. (2-3), pp (86-92)

[20] Han, Y.; Lin J. and Zhang H. (2002). Photoluminescence of organic-inorganic hybrid SiO$_2$ xerogels, *Mat. Lett.*, Vol. 54, No. (5-6), pp (389-396)

[21] Gu G.; Ong P.P. and Chu C. (1999). Thermal stability of mesoporous silica molecular sieve, J. *Phys. Chem. Sol.*, Vol. 60, No. 7, pp (943-947)

[22] García M.; Mondragón M.A.; Téllez S.; Campero A. and Castano V.M. (1995). Blue emission and tetraethoxysilane and silica gels, *Mater. Chem. Phys.*, Vol. 41, No. 1, pp (15-17).

[23] Moulder, J.F.; Stickle, W.F.; Sobol, P.E. and Bomben, K. (1992). *Handbook of X-ray photoelectron spectroscopy*, Perkin Elmer Corp., Minnesota (USA).

[24] Carriere, B. and Lang, B. (1977). A study of the charging effect and dissociation of SiO$_2$ surfaces by AES, *Surf. Sci.*, Vol. 64, pp (209-223)

[25] Fiori, C. and Devine, R.A.B. (1984). Photon-induced oxygen loss in thin SiO$_2$ films, *Phys. Rev. Lett.*, Vol. 52, No. 23, pp (2081-2083)

[26] Blasse, G.; Grabmaier, B.C. (1994). *Luminescent Materials*, Springer Verlag, ISBN 3-540-58019-0 New York

[27] Solé, J.G.; Bausá, L.E.; Jaque D. (200). *An Introduction to the Optical Spectroscopy of Inorganic Solids*, John Wiley and Sons, Ltd, ISBN 0-470-86886-4,Chichester.

[28] Mhlongo, G.H.; Ntwaeaborwa, O.M., Dhlamini, M.S.; Swart, H.C; Hillie, K.T. (2011a). Effects of Ce^{3+} concentration, beam voltage and current on the cathodoluminescence of intensity of SiO$_2$:Ce^{3+}-Pr^{3+} nanophosphor, J. Alloy. Compd., Vol. 509, pp (2986-2992)

[29] Sokólska, I.; Golab, S.; Baluka, J.; Ryba-Romanowski, W. (2000), Quenching of Pr^{3+}in single crystals of K$_5$Pr$_x$La$_{1-x}$Li$_2$F$_{10}$., *J. Lumin.*, Vol. 91, pp (79-86).

[30] Mhlongo, G.H.; Ntwaeaborwa, O.M., Swart, H.C.; Kroon, R.E.; Solarz, P.Ryba-Romanowski, W., Hillie, K.T. (2011b). Luminescence dependence of Pr^{3+} activated SiO$_2$ nanophosphor on Pr^{3+}concentration, temperature and ZnO incorporation, *J. Phys. Chem. C.*, Vol. 115, pp (17625 – 17632).

[31] Mhlongo, G.H.; Ntwaeaborwa, O.M.; Dhlamini, M.S.; Swart, H.C.; Hillie, K.T. (2010) Cathodoluminescence properties of SiO$_2$:Pr^{3+} and ZnO·SiO$_2$:Pr^{3+}, *J. Mater. Sci.*, Vol. 45, pp (5228 – 5236).

[32] Kumar, V.; Mishra, V.; Pitale, S.S.; Nagpure, I.M.; Coetsee, E.; Ntwaeaborwa, O.M.; Terblans, J.J.; Swart, H.C. (2010). Surface chemical reactions during electron beam irradiation of nanocrystalline CaS:Ce^{3+} phosphor, *J. Appl. Phys.*, Vol. 107, pp (123533-1 - 123533-6)

[33] Bol, A.A.; Meijerink, A. (2001). Luminescence of nanocrystalline ZnS:Pb^{2+}, *Phys. Chem. Chem. Phys.*, Vol. 3 (11), pp (830-832).

[34] Ntwaeaborwa, O.M.; Kroon, R.E.; Kumar, V.; Dubroca T.; Ahn, J.-P.; Park, J.-K.; Swart, H.C. (2009a), Ex-situ synthesis and optical properties of ZnO-PbS nanocomposites, *J. Phys. Chem. Sol.*, Vol. 70, pp (1438 – 1442)

[35] Ntwaeaborwa O.M.; Swart H.C.; Kroon, R.E.; Terblans, J.J.; Holloway, P.H. (2009b). Synthesis, characterization and luminescent properties of ZnO-SiO$_2$:PbS, *J. Vac. Sci. Technol. A.*, Vol. 27(4), pp (767 – 769)
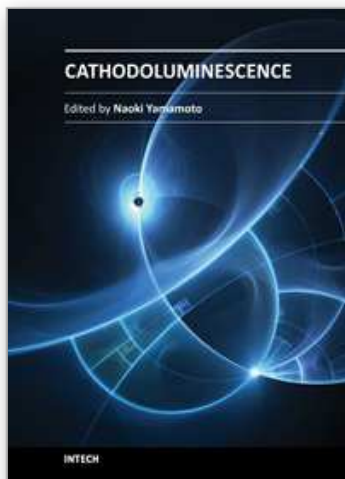
Cathodoluminescence

Edited by Dr. Naoki Yamamoto

Cathodoluminescence (CL) is a non-destructive technique to characterize optical and electronic properties of nanostructures in many kinds of materials. Major subject is to investigate basic parameters in semiconductors, impurities in oxides and phase determination of minerals. CL gives information on carrier concentration, diffusion length and life time of minority carriers in semiconductors, and impurity concentration and phase composition in composite materials. This book involves 13 chapters to present the basics in the CL technique and applications to particles, thin films and nanostructures in semiconductors, oxides and minerals. The chapters covered in this book include recent development of CL technique and applications to wide range of materials used in modern material science.

INTECH
open science | open minds